Structures, Structural Dynamics, and Materials and Co-located Conferences
April 8-11, 2013, Boston, Massachusetts
54th AIAA/ASME/ASCE/AHS/ASC Structures, Structural Dynamics, and Materials Conference

Navier-Stokes based Unsteady Aerodynamic Computations of Launch Vehicles undergoing Forced Coupled Oscillations

Guru Guruswamy*
NASA Ames Research Center, Moffett Field, CA, 94035 U.S.A.

A procedure is presented to accurately model transient motions of launch vehicles associated with complex flow conditions. The flow is modeled using the Reynolds-Averaged Navier-Stokes equations with the one-equation Spalart-Allmaras turbulence model. An overset grid system with a curvilinear near-body grid and a Cartesian off body is used. Solution quality is assessed using grid sensitivity and time-step convergence studies. Validation computations are made for a clean configuration model of the Saturn V launch vehicle for rigid-body transient motions in both the longitudinal and lateral directions, which are typically encountered during launch vehicle ascent. The effect of these transient motions on the unsteady aerodynamic response is studied. Unsteady aerodynamic response surfaces are efficiently computed using a massively parallel computer system.

Nomenclature

A	=	sectional area at maximum diameter in ft^2
c_p	=	coefficient of pressure
c_{pr}	=	coefficient of pressure in radial direction
c_{px}	=	coefficient of pressure in longitudinal direction
Cn	=	coefficient of total lateral force
C_x	=	coefficient of total longitudinal force
D	=	maximum diameter in ft
f	=	oscillating frequency in cycles per second
h	=	lateral displacement
H	=	amplitude of lateral motion
k	=	reduced frequency, $\omega D/U$
L	=	length of the vehicle in ft
M_∞	=	free stream Mach number
r	=	radial coordinate
Re_D	=	Reynolds number based on D
U	=	speed in ft/sec
v	=	longitudinal displacement
V	=	amplitude of longitudinal displacement
x	=	roll axis along longitudinal direction
y	=	yaw axis along 0 circumferential angle
z	=	axis perpendicular to x-y plane
t	=	time in seconds
ω	=	$2\pi f$, circular frequency in radians/sec
Φ	=	phase lead of lateral motion with respect to longitudinal motion matrix
θ	=	circumferential angle with respect to vertical plane of symmetry on the windward side

---

*Sr. Scientist, Fundamental Modeling and Simulation Branch, AIAA Associate Fellow

I. **Introduction**

Launch vehicles pass through various flow regimes during flight and often undergo significant flow-induced structural oscillations. For example, propulsion-structure interactions can introduce significant longitudinal oscillations in the launch vehicle, which in turn can introduce lateral oscillations [1]. Lateral oscillations can also be introduced due to transonic buffet [2]. Such oscillations can adversely affect performance and can lead to aeroelastic instabilities [1].

Typically, the external aerodynamic lines of a launch vehicle are axisymmetric. Internally, they contain mass and structural elements that are not axisymmetric. If these asymmetries are small, the oscillatory modes can be treated as uncoupled. Occasionally, this simplification is not permissible because the mass and structural asymmetries are significant. This leads to strong coupling between the longitudinal and lateral modes with correspondingly large aerodynamic loads. Strong coupling of lateral and longitudinal oscillations occurred for the Saturn V launch vehicle [3]. Such transient coupling results in aeroelastic deformations and can affect launch vehicle performance [4]. Coupled oscillations can also occur due to flow asymmetries.

Accurate methods to compute unsteady airloads resulting from coupled lateral/longitudinal oscillations are needed for the safe design of launch vehicles. General-purpose codes such as NASTRAN [5] can compute unsteady airloads associated with complex geometries using the linear doublet lattice and Mach box methods for subsonic and high supersonic flows, respectively [6]. However, linear aerodynamic methods cannot model flow nonlinearities, as demonstrated in [7] for the ARES launch vehicle. This is especially true in the transonic and low supersonic speed regimes due to the existence of many nonlinear flow features, e.g., viscous effects, shock/boundary layer separation, and flow buffeting.

The Reynolds-Averaged Navier-Stokes (RANS) equations are already in widespread use to model flow non-linearities of launch vehicles [8,9]. To date the majority of RANS-based computations for launch vehicles have been limited to steady and unsteady flows over non-moving rigid-body configurations. Demonstration computations applied to moving body configurations using the Euler equations were presented in [10], but did not include validation using unsteady data. Recently, an effort to compute unsteady flows on an oscillating configuration using linear theory with mean-flow corrections computed from the RANS equations was presented in [11]. Such methods may work for moderate flow non-linearity, but are generally not adequate when strong flow non-linearity exists due to moving shock waves [12]. The need for RANS methods to accommodate flow non-linearity for launch vehicle simulations has been suggested by a number of researchers, e.g., see Ref. 13.

The purpose of this paper is to demonstrate a validated procedure to accurately compute unsteady flows associated with the oscillatory motions of launch vehicles such as NASA's current Space Launch System Project [14]. Validation computations are made for a clean configuration model of the Saturn V launch vehicle [15] undergoing coupled longitudinal and lateral rigid-body oscillations. The OVERFLOW computer code [16] solving the RANS equations with the Spalart-Allmaras (SA) turbulence model [17] and an overset grid approach [18] is used for all computations. Results are compared with measured steady pressures [19, 20] and computed linear unsteady aerodynamic forces [21]. The forced motions are prescribed based on existing data from the flight model [22]. The large computer time needed to compute unsteady flows on the oscillating configurations is efficiently addressed using parallel computational protocols developed for super clusters [23].

II Saturn V Model

Since validation data is available for the Saturn V launch vehicle [13] (clean configuration shown in Fig. 1), it is used here as a suitable test geometry. The Saturn V is the largest and most powerful rocket flown to date. It was 363 feet tall with a maximum diameter of 33ft and possessed a lift-off weight of 6.2 million pounds. It could boost 291200 lbs into Earth orbit and 112000 lbs to the moon.

The Saturn V configuration faced several technical challenges that are important in the context of the present study. During launch it experienced significant flow induced oscillations [1, 3]. Unsteady cavitational flows triggered longitudinal oscillations known as the "POGO" effect, which in turn induced lateral oscillations [1]. This phenomenon started at about 40 seconds after launch (t = 40 sec) where the freestream Mach number (M_∞) was about 0.6 and continued until t = 150 sec, $M_\infty = 3.5$.

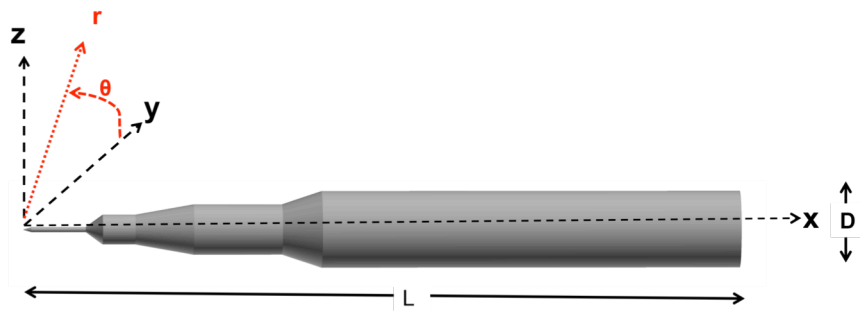

Fig. 1 Model of the Saturn V launch vehicle without protuberances and propulsion system.

NASA is now embarking on the design of a next-generation heavy launch vehicle known as the Space Launch System (SLS) [14] that will support the Agency's future large-scale science and exploration missions. Potential future missions include trips to near-Earth objects, such as asteroids, lunar missions, scientific research missions, and human exploration missions to Mars. In this context it is important to use high fidelity tools that can accurately compute flows associated with vehicle oscillations to help understand and alleviate the undesirable impact of this dangerous phenomenon on performance and safety. In this paper accurate flow simulations are performed using the unsteady RANS equations with a state-of-the-art turbulence model.

II Flow Solver

The OVERFLOW flow code [16] is used to solve the time-dependent RANS equations in the context of an overset grid approach that consists of both curvilinear and Cartesian grid zones. The code has a variety of implicit and relaxation algorithms that utilize a variety of upwind and central spatial differencing schemes. Both global and Newton sub-iteration time-stepping options are available. A variety of zero, one, and two-equation RANS or hybrid RANS/LES turbulence models including the popular DES (detached eddy simulation) model are available. A more complete description of the OVERFLOW CFD code and its user's manual can be found in Refs. 16 and 24. In the present study computations are made using a fifth-order accurate spatial scheme with the one equation SA [17] turbulence model. The spatial scheme used is actually a 6^{th} order central scheme for the convective terms with a 5^{th} order dissipation scheme, which results in 5^{th} order accuracy. The viscous terms are handled with a 2^{nd} order central scheme, and the metrics are also handled with a 2^{nd} order central scheme. Time advance uses the Pulliam-Chaussee [25] diagonalized version of the Beam-Warming ADI scheme [26] with a dual time-stepping approach for 2^{nd} order temporal accuracy.

III Grid

The OVERFLOW flow solver utilizes a robust overset grid capability with provisions for prescribing moving rigid bodies. In the present effort two grid systems are utilized: a curvilinear near-body (NB) grid, which is fitted to the aerodynamic surface of interest, and an off-body (OB) grid that is Cartesian in construction and completely surrounds the NB grid. Figure 2 shows a portion of the resulting grid system near the Saturn V configuration. Specifically, this grid was based on the full-configuration grid presented in Ref. 26, which was generated using the OVERGRID grid generation software tool [16, 26]. Accepted time-tested engineering practices [16, 26] are followed in generating the best possible grid. The NB grid has 763 axial, 89 circumferential and 84 radial grid points. It has a spherical topology with an axis of singularity emanating from the nose and the rocket base. The wall normal spacing at the surface of the body is 25.0×10^{-6} of the maximum diameter (D). The NB grid outer boundary is located at about 0.12L away from the vehicle surface. The OB grid has 243X171X171 grid points in the x, y, z directions, respectively, with an outer boundary located at about 7.5L away from the vehicle surface. The total number of grid points in the NB and OB grid systems is 12809751.

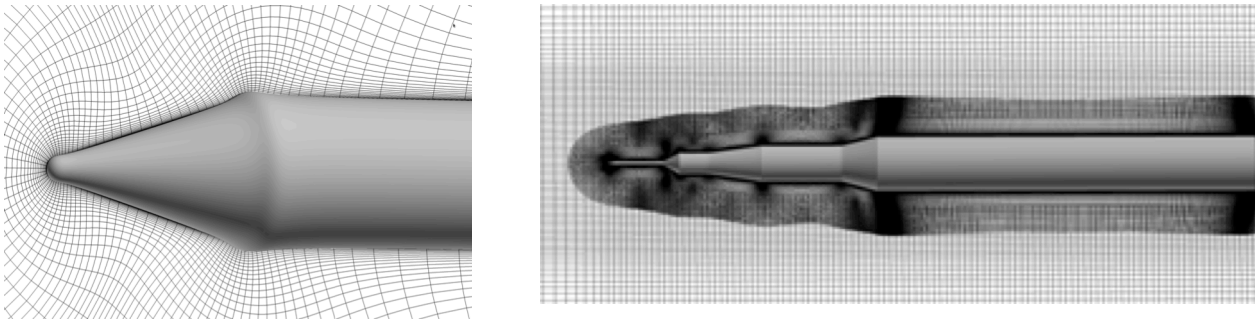

(a) Grid blowup near the launch vehicle nose (b) Entire NB grid with a portion of the OB grid

Fig. 2 Two grid system used for the Saturn V launch vehicle (clean configuration)

III Validation

A. Grid Quality Assessment with Steady State Computations

To study grid quality, a supersonic case, lying within the launch trajectory range where oscillations occurred, has been selected (M_∞ = 1.80 and Re_D = $2.2x10^6$). Steady state experimental data [20] and linear-theory-based unsteady aerodynamic data [21] are available for comparisons. An initial set of steady-flow computations, each run for 5000 steps, are performed first, using a variable time-step option in OVERFLOW without sub-iteration. As recommended by the NPARC Alliance (National Program for Applications-Oriented Research in CFD) [27] for Applied CFD computations, the integrated axial force coefficient, C_x, is monitored for convergence. C_x is defined as

$$C_x = \frac{1}{A}\int_0^L \int_0^{2\pi} c_{px}\, d\theta dx \qquad (1)$$

where c_{px} is the x-direction component of the pressure coefficient c_p, θ is the angle in the circumferential direction and A (= $0.25\pi D^2$) is the cross-sectional area. As seen in Fig. 3 C_x converges in about 3000 steps for a typical steady-state case.

Next, a grid sensitivity study is performed to assess grid quality. At M_∞ = 1.80 and Re_D = $2.2x10^6$ the NB grid, as described above, yields an average y^+ value (one point off the aerodynamic surface) of 1.18, which is typically adequate to resolve the boundary layer skin friction. A study to determine the effect of the outer boundary position on the solution is preformed next by systematically changing the outer boundary position of the OB grid simultaneously in both the y and z directions from 0.25L to 12.07L. The corresponding variation in the number of grid points is 682587 to 7960923 points for the OB grids and 6326K to 14110K points for the total grid. Computations are performed on each grid for 5000 iterations, producing a convergence history similar to that shown in Fig. 3. Figure 4 shows a plot of Cx for this set of grids versus outer boundary position. Results converge for an outer boundary position near 3.0L. Therefore, the original grid with an outer boundary position at 7.54L is deemed adequate for the present study.

To study adequacy of the grid in the axial direction, computations are made using a series of NB grids with increased spacing in x-direction—double the spacing (384 points), and quadruple the spacing (195 points)—while keeping the OB grid the same. This is accomplished by modifying the baseline NB grid (763 points) using the cubic spline interpolation option available in the SRAP module of OVERGRID [18]. An additional computation is made on a finer OB grid (1049 points), which was generated using OVERGRID and reported in Ref. 27. All sharp corners for all grids are retained. Figure 5 shows the effect of the NB grid refinement in the x-direction on Cx. As seen, the baseline grid (763 points in the x-direction) produces a value of Cx in close agreement (difference ~ 0.8%) with the finer 1049-point grid.

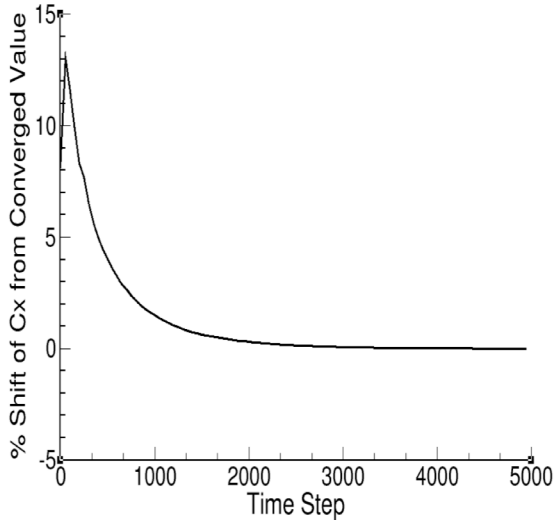

Fig. 3 Steady-state convergence of C_x with iteration at $M_\infty = 1.80$ and $Re\_D = 2.2x10^6$.

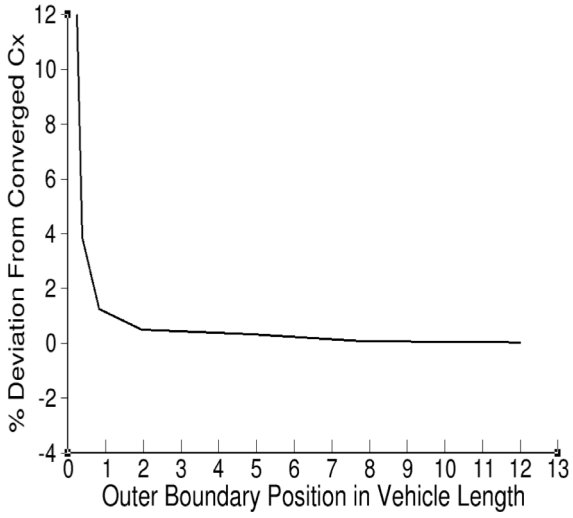

Fig. 4 Effect of outer boundary position on steady state C_x at $M_\infty = 1.80$ and $Re\_D = 2.2x10^6$.

Figure 6 shows a comparison of c_p between the four grids used in the Fig. 5 grid sensitivity study and experiment [20]. Within engineering scale all grids compare well with the experiment. Solution for grids with 195 and 384 deviate slightly at peaks from that for grid with 1049 points. The baseline grid (763) and the fine grid (1049) compare well with each other. For both grids except for local differences around x/D = 1.0 and 2.5, all of which are small, the comparison with experiment is good. The fact that the baseline grid was generated using the advanced grid generation tool OVERGRID with widely accepted engineering practices and convergence behavior shown in Figs. 3 to 5, demonstrates that this grid is adequate for the computations presented in this paper. For all further calculations the baseline grid with NB = 5704108 points and OB = 7105563 points will be used.

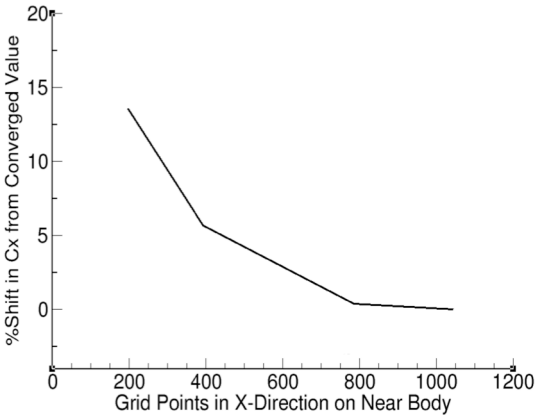

Fig. 5 Effect of the NB x-grid distribution on axial force coefficient error at $M_\infty = 1.80$ and $Re\_D = 2.2x10^6$.

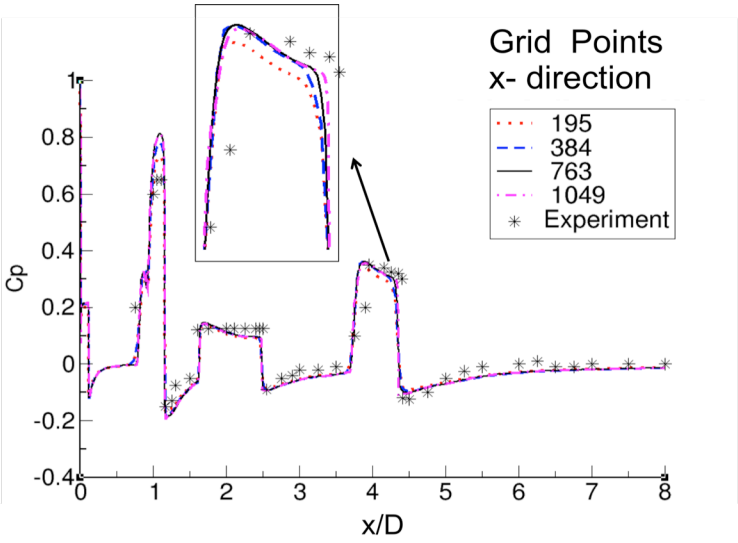

Fig. 6 Pressure coefficient (cp) comparisons between computation and experiment [30] at $M_\infty = 1.80$ and $Re\_D = 2.2x10^6$.

B. Oscillatory motions

Motions for the unsteady computations are computed using

$$v = V \sin(\omega t) \tag{2}$$

$$h = H \sin(\omega t + \Phi) \tag{3}$$

where v and h are instantaneous longitudinal and lateral rigid-body displacements obtained from corresponding amplitudes, V and H, respectively. The time in seconds and oscillatory frequency in radians per second are represented by t and ω, respectively. The symbol Φ denotes phase lead/lag of the lateral motion with respect to longitudinal motion. The reduced frequency k is defined as $\omega D/U_\infty$ where U_∞ is the free stream velocity.

Based on published data [3] the typical average longitudinal frequency of the Saturn V launch vehicle during its oscillation phase was ~5.25 Hz. This produces a range of k = 2.2 to 0.30 for M_∞ ranging from 0.5 to 3.5. The peak oscillation amplitude occurred at $M_\infty \sim 2.2$, which corresponds to k ~ 0.50. In this paper all computations are made for k = 0.50. The oscillation amplitudes for the Saturn V launch vehicle have not been published. In this effort it is assumed that the maximum amplitude for both longitudinal and lateral motions is 0.5% of L.

C. Unsteady Computations

The Saturn V launch vehicle experienced a number of undesirable oscillations during launch, which were not documented. Hence, data associated with these phenomena, including unsteady pressures, are not available for validation [19-20]. As a result, solution validation is accomplished in the present paper using numerical experiments and comparisons with other well-established numerical results, for example, unsteady aerodynamic results based on linear potential theory that are valid for high supersonic Mach numbers [19]. A case at $M_\infty = 1.80$ and Re_D = 2.2×10^6 has been selected for validation.

Unsteady computations are presented next to show how mean unsteady pressures compare with steady-state pressures. To start, unsteady computations are made at $M_\infty = 1.80$ for V = 0.005L, H = 0.0 and k = 0.5 with a variable number of steps per cycle (NSPC). It was found that NSPC = 2400 produced a stable solution without using Newton subiterations (NWIT). The rest of the time step convergence studies are made using NSPC = 2400.

Since Newton iterations are required to maintain 2nd order time accuracy, the next study involved the variation of NWIT. Computations are made for 4 cycles with increasing NWIT. Figure 8 shows plots of C_x for NWIT = 5, 10, 15 and 20. The solutions during the first cycle of the computation have not achieved periodic behavior and should not be quantitatively evaluated. The solutions for cycles 2-4 are reasonably periodic. They contain high frequency components of small amplitude in addition to the largest unsteady component at the forcing frequency. Only small variations are induced in the solution due to the number of subiterations utilized, especially when NWIT is larger than 10.

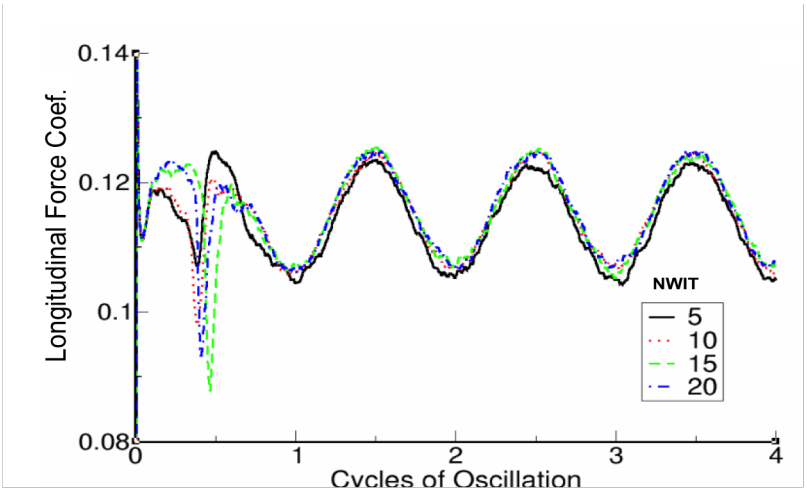

Fig. 8 Unsteady C_x due to longitudinal oscillations for V = 0.005L, H = 0.0, $M_\infty = 1.80$, k = 0.5 and Re_D = 2.2×10^6.

Figure 9 shows results of Fourier analysis for the component corresponding to the forcing frequency (k = 0.50) of the responses of Fig. 8. Results are scaled by the amplitude H. Note that the dominant frequency is clearly the forcing frequency and that all responses for NWIT ≥10 are nearly identical. For all remaining computations NWIT = 20 is used.

As a check on unsteady solution correctness, time-averaged unsteady pressures are compared next with steady-state pressures in Fig. 10. The two unsteady computations are made with H = 0.005L, V = 0.0 and with H = 0.005L, V = 0.005L. As expected, the time-averaged pressures are smoothed near peaks but close to steady-state values.

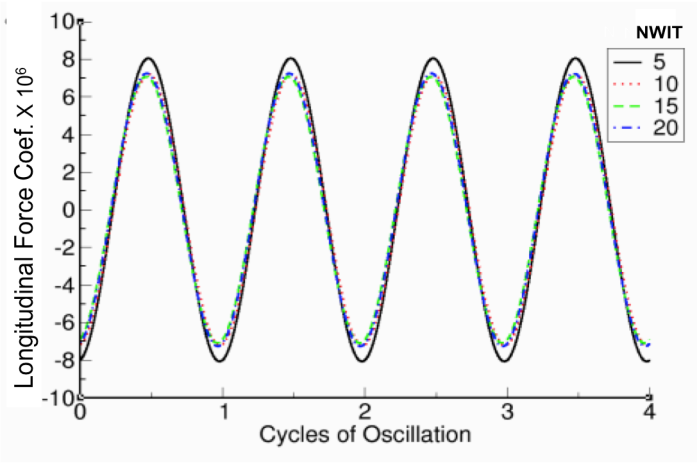

Fig. 9 Fourier coefficient of unsteady C_x at forcing frequency for V = 0.005L, H = 0.0, k = 0.5 and Re_D = 2.2×10^6.

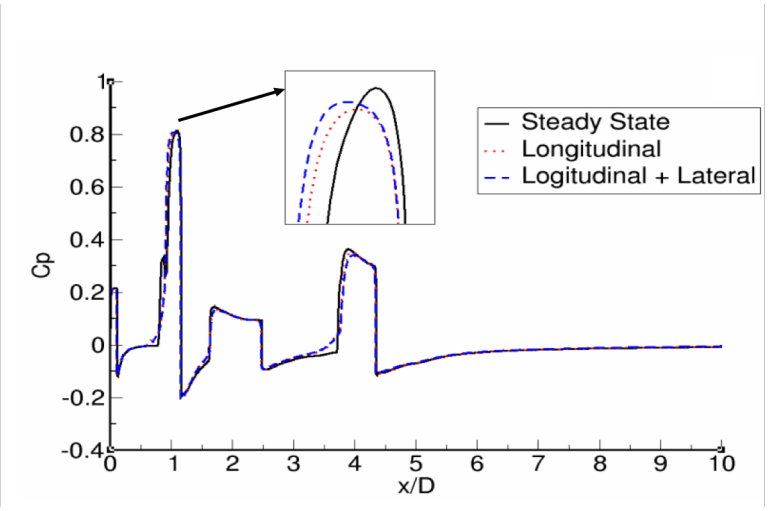

Fig. 10 Comparison of time-averaged unsteady pressures with steady-state pressures at M_∞ = 1.80 and Re_D = 2.2×10^6.

Unsteady computational results are compared next based on the indicial approach [21], using both linear aerodynamics and OVERFLOW. First, a response is computed for a step-change in angle-of-attack of 1.0 deg. Figure 11 shows the resulting response in the lateral force coefficient (Cn) over a non-dimensional time ωt of 80 radians. C_n is defined as

$$Cn = \frac{1}{A}\int_0^L \int_0^{2\pi} c_{pr} \mathrm{Cos}\theta d\theta dx \qquad (4)$$

where c_{pr} represents component of c_p in the radial direction.

Next, Duhamel integration [29] is performed on the indicial response to compute frequency domain data. Figure 12 shows a comparison (multiple amplitudes at various reduced frequencies) for both the linear aerodynamic theory and OVERFLOW approaches. Agreement is reasonable with some shifts in magnitude and phase for reduced frequencies up to 1.6, which are within the practical values for launch vehicles.

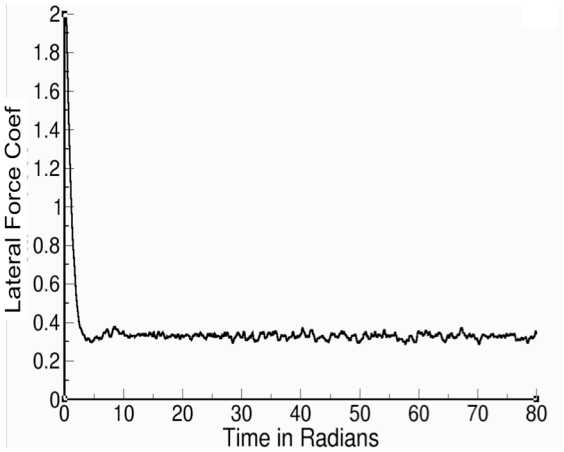

Fig. 11 Indicial response lateral force for 1 deg step change in angle of attack at $M_\infty = 1.80$.

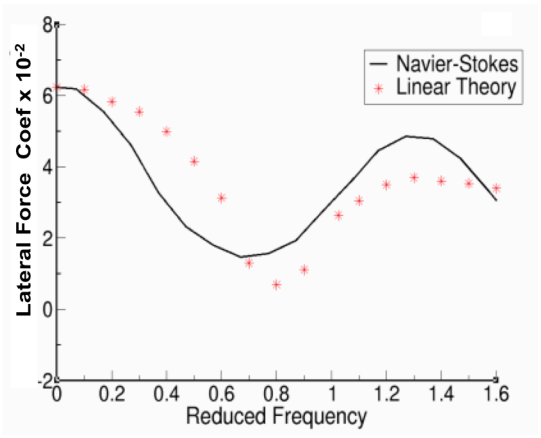

Fig. 12 Comparison of RANS results with linear aerodynamic theory [21].

D. Effect of Lateral Displacement.

As reported in [30] longitudinal oscillations induced lateral oscillations. Thus, it is of interest to see the effect of lateral motions on unsteady aerodynamic forces. Computations are made for 5 cycles at $M_\infty = 1.80$, V = 0.005L, while H varied from 0.0 to 0.005L in increments of 0.001L. As shown in Fig. 13, axial force amplitudes are not dramatically affected by changing lateral displacement amplitude, but the phase angle does change, especially for $H \geq 0.004L$.

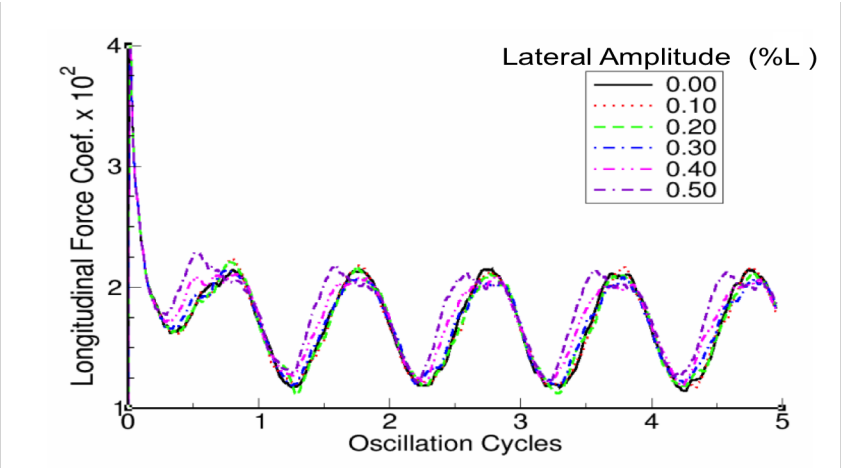

Fig. 13 Effect of lateral oscillation on unsteady C_x for $M_\infty = 1.80$, H = 0.005L and varying V.

Figure 14 shows the effect of lateral displacement amplitude (H) on the lateral force response. As can be seen, the increase in force amplitude is nearly linear with increasing lateral displacement amplitude. Phase angles remain

almost constant. In addition, the amplitudes associated with higher frequency components in the lateral force response appear to decrease with increasing lateral displacement amplitude.

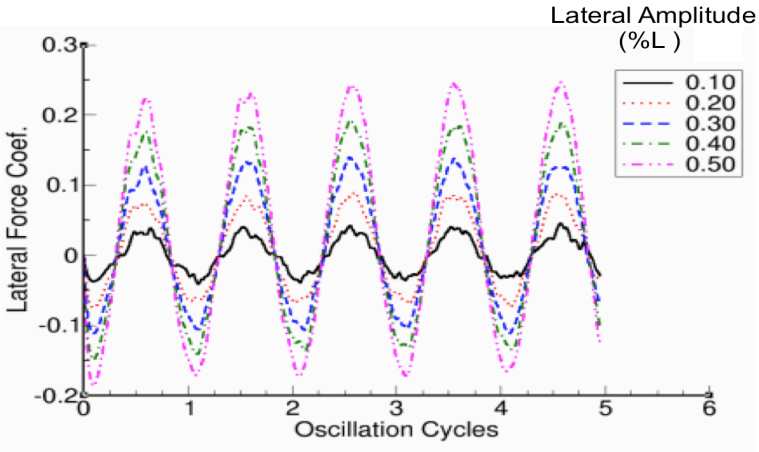

Fig 14 Effect of lateral oscillation on unsteady $C_{n\ for}$ $M_\infty = 1.80$, H = 0.005L and varying V.

An instantaneous snap shot of surface pressure contours from the unsteady OVERFLOW solution (V = 0.005L, H = 0.005L and k = 0.50) at maximum h and v values is shown in Fig. 15. Circumferential flow variations are pronounced in regions where the diameter changes rapidly in the axial direction. Localized, high-frequency flow unsteadiness is also largest in these locations. Flow asymmetry at maximum displacements can be seen near x/D = 2.5 in Fig. 15.b.

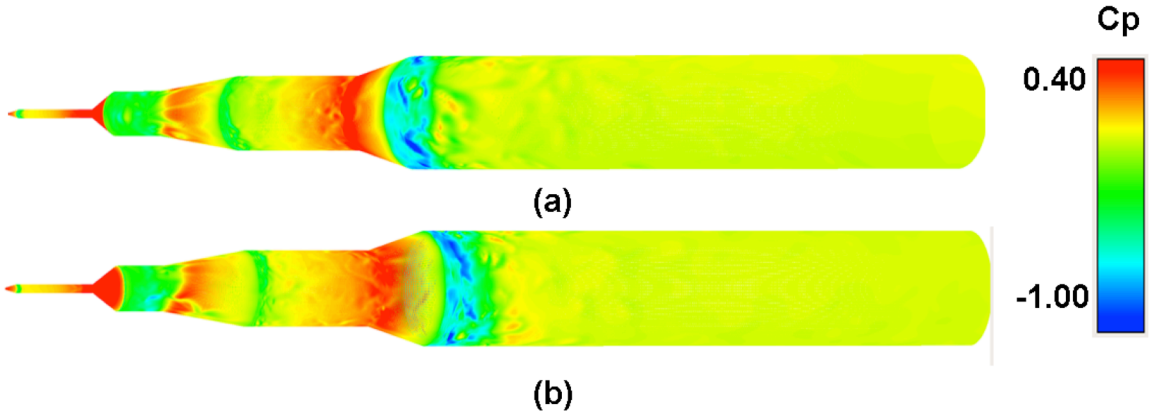

Fig. 15 Instantaneous snap shot of unsteady pressure contours on the Saturn V launch vehicle taken from the OVERFLOW solution (V = 0.005L, H = 0.005L, k = 0.5, M_∞ = 1.8, Re_D = 2.2×10^6) when h and v are maximum.
a) h = 0, v = 0; b) h = 0.005L, v = 0.005L.

E. Effect of Mach number

Oscillations for the Saturn V launch vehicle occurred over a range of Mach numbers from high subsonic to high supersonic. In this section effects of freestream Mach number on the longitudinal and lateral forces are determined using 84 individual computations with 0.025 increments in M_∞ ranging from 0.9 to 2.975 (~3.0). This is a massive computation that needs a significant amount of computer time. It is efficiently implemented using a parallel execution-script called RUNDUA [31] to submit a large number of individual cases in a single job environment on the Pleiades super cluster associated with the NASA Advanced Supercomputing (NAS) Facility [32, 23].

In this effort two separate RUNDUA jobs, each consisting of 42 cases, were run. Each case was assigned to 80 processors requiring a total of 3360 cores for each 42-case job. All cases were run for 5 cycles with 2400 steps per cycle and NWIT = 20. Each 42-case job required a total 25 hrs of wall clock time. All 84 cases combined generated about 1.1million unsteady surface data points, which produced about 7 Terabytes of data.

A carpet plot showing the longitudinal force response for the 5th oscillation cycle is shown in Fig. 16. For all Mach numbers, peaks in the longitudinal force coefficient occur near minimum displacement. The rate of change of C_x with respect to M_∞ varies with displacement.

A carpet plot showing the lateral force coefficient for the 5th oscillation cycle is shown in Fig. 17. Mach number has a stronger impact when the displacements are near the maximum and minimum peaks. Responses are more sensitive at lower Mach numbers (~1.2).

Plots like those shown in Figs. 16 and 17 can be generated for different combinations of motions and angles of attack as needed for design. The current version of OVERFLOW has limited capabilities to model flexible configurations such as 1-D rotorcraft blades [33]. Once general structural flexibility is added to OVERFLOW, the present procedure can include aeroelastic effects from the lateral modes [34].

VI Conclusions

A procedure based on solving the Reynolds-Averaged Navier-Stokes equations is presented for computing the unsteady aerodynamic loads of launch vehicles undergoing various longitudinal and lateral oscillations that are typically encountered during launch. Steady flow computed results are verified using a number of numerical experiments and validated using experimental data. Due to lack of measured data unsteady computed results are verified using numerical experiments and the linear aerodynamic theory. Comparison between current results and the linear aerodynamic theory is good at a free-stream Mach number of 1.8 where flow characteristics are linear. The time-averaged unsteady pressures compare well with steady pressures. Lateral motions produce an influence on longitudinal forces for lateral displacement amplitudes higher than about 0.4% of the length of the vehicle. Effect of lateral displacements on lateral forces is almost linear for amplitudes up to 0.5% of length. Use of massively parallel computations makes it practical to generate a large number of cases within a single day. Five-cycle responses for 42 Mach numbers are obtained in 25 hrs of wall clock time using 3360 cores. The present procedure provides a foundation to accurately compute unsteady aerodynamic forces that arise in aeroelasticity of launch vehicle flight configurations.

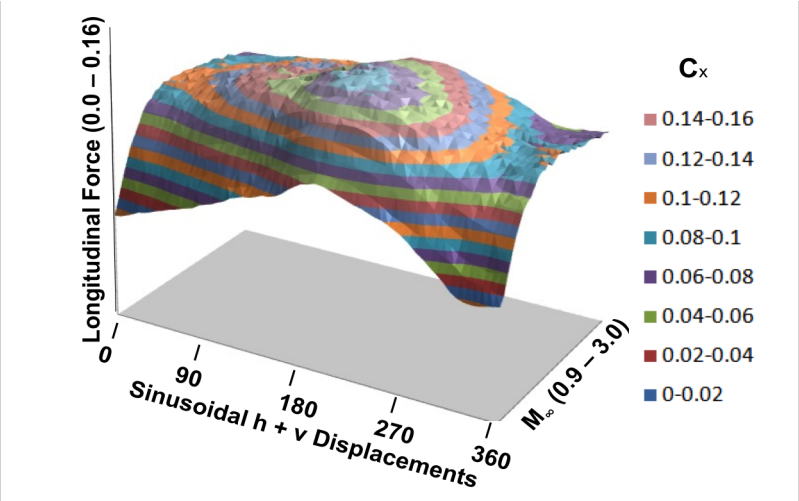

Fig. 16 Effect of Mach number on longitudinal forces at 5th cycle.

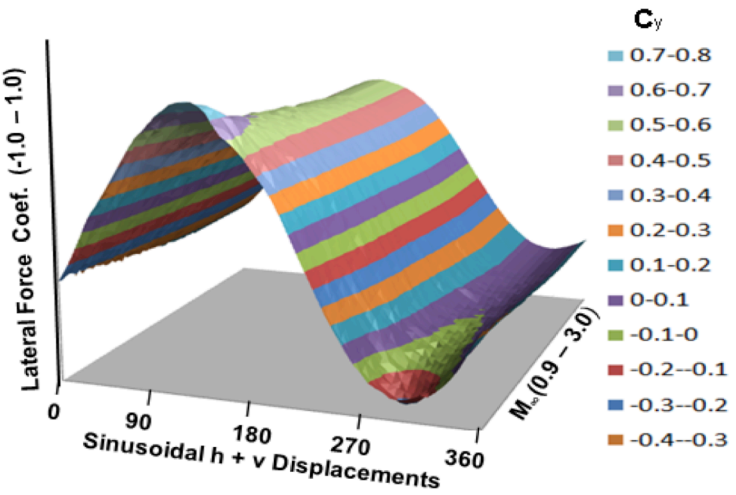

Fig. 17 Effect of Mach number on lateral forces for 5th cycle.

Acknowledgements

The author thanks Shishir Pandya and William Chan of NASA Ames Research Center for providing consultations on grid data for Saturn V vehicle and OVERGRID software. Valuable suggestions by Terry Holst, Chief of Fundamental Modeling and Simulation Branch of Ames Research Center, are appreciated. This effort is funded under the High End Computing project of the NASA Advanced Supercomputing Division (NAS).

References

1. "Prevention of Coupled Structure-Propulsion Instability (POGO)," NASA SP-8055, Oct. 1970.
2. Hanson, P. W., and Doggett, R. V., "Aerodynamic Damping and Buffett Response of an Aeroelastic Model of Saturn I block Launch Vehicle," NASA TN-D2713, March 1965.
3. Ryan, R. S, Papadopoulos, J. G., Kiefling , L., Odum, R., Jarvinen, W., and Kennoy, J., "A Study of Saturn AS-502 Coupling Longitudinal Vibration and Lateral Bending Response during Boost," AIAA Paper 1969-58, AIAA 7th Aerospace Sciences Meeting, New York, Jan. 1969.
4. Dotson, K. W., "Transient Coupling of Launch Vehicle Bending Responses with Aerodynamic Flow State Variations," *J. of Spacecraft and Rockets*, Vol. 38, No. 1, 2001, pp. 97-104.
5. "NASTRAN User's Manual," NASA SP-222 (08), June 1986.
6. Foist, B. L., Grau, E. L., and Nejad, B. I., "Launch Loads Development Using Sine Vibration Methodology," AIAA Paper 2004-1800, April 2004.
7. Orr, J., "A Coupled Aeroelastic Model for Launch Vehicle Stability Analysis," AIAA Paper 2010-7642 AIAA Atmospheric Flight Mechanics Conference, Toronto, Ontario, Aug. 2010.
8. Engblom, W. A., "Numerical Simulation of Titan IVB Transonic Buffet Environment," *J. of Spacecraft and Rockets,* Vol. 40, 2003, pp. 648–656.
9. Pao, S., Vatsa, V., Abdol-Hamid, K., Pirzadeh, S., Klopfer, G., and Taft, J.R. and Parlette, E., "Best Practice for Ascent Aero Analysis for the Ares I Configurations," JANNAF-55, 2008.
10. Kleb, W. L., "Aerodynamic Characteristics of Aerospace Vehicle during a Subsonic Pitch-Over Maneuver," AIAA Paper 96-0825, April 1996.
11. Capri, F., Mastroddi, F., and Pizzicaroli, A., "Linearized Aeroelastic Analysis for a Launch Vehicle in Transonic Flight," *J. of Spacecraft and Rockets*, Vol. 43, No. 1, 2006, pp. 92–104.
12. Guruswamy, P. and Yang, T.Y., "Aeroelastic Time Response of Thin Airfoils by Transonic Code LTRAN2," *Computers and Fluids,* Vol. 9, No. 4, 1981, pp. 409-425.
13. Dotson, K. W. and Tiwari, S. B, "Formulation and Analysis of Launch Vehicles Maneuvering Loads," *J. of Spacecraft and Rockets*, Vol. 33, No. 6, Nov-Dec. 1996, pp. 815-821.

14. NASA Space Launch System (http://www.nasa.gov/exploration/systems/sls/) (Date accessed Feb 7, 2013)
15. .http://www.nasa.gov/audience/foreducators/rocketry/home/what-was-the-saturn-v-58.html(Date accessed Feb 7, 2013).
16. Nichols, R. H., Tramel, R. W., and Buning, P. G., "Solver and Turbulence Model Upgrades to OVERFLOW 2 for Unsteady and High-Speed Applications," AIAA Paper 2006-2824, AIAA 36th Fluid Dynamics Conference, San Francisco, CA, June 2006.
17. Spalart, P. R. and Allmaras, S. R., "A One-Equation Turbulence Model for Aerodynamic Flows," AIAA Paper 92-0439, Jan. 1992.
18. Chan, W. M., "Developments in Strategies and Software Tools for Overset Structured Grid Generation and Connectivity," AIAA Paper 2011-3051, 20th AIAA Computational Fluid Dynamics Conference, Honolulu, Hawaii, June 2011.
19. Brice, T. R. and Robertson, J. E., " Pressure Test on a 0.04 Scale Model of the Saturn V Launch Vehicle at Mach numbers from 0.60 through 1.45," AEDC-TR-66-217, Nov. 1966.
20. Brice, T. R. and Robertson, J. E., "Pressure Test on a 0.04 Scale Model of the Saturn V Launch Vehicle at Mach numbers from 1.8 through 3.00," AEDC-TR-67-217, June 1967.
21. Glauz, W. D. and Blackburn, R. R, "Study of Indicial Aerodynamic Forces on Multistage Space Vehicle Systems - Volume I - Application of Theory to Basic Geometries and to the Saturn V," NASA CR 61928, Sept. 1968.
22. Pinson, D. P. and Lonard, H. W., "Longitudinal Vibrations Characteristics of Apollo/Saturn V Replica Model," NASA TN D-5159, April 1969.
23. Guruswamy, G. P., "Large-Scale Computations for Stability Analysis of Launch Vehicles Using Cluster Computers," *J. of Spacecraft and Rockets*, Vol. 48, no 4, July-Aug. 2011, pp 584-588.
24. Nichols, R. and Buning, P., "User's Manual for OVERFLOW 2.1," University of Alabama at Birmingham, Birmingham, AL, 2008.
25. Pulliam, T. H. and Chaussee, D. S., "A Diagonal Form of an Implicit. Approximate-Factorization Algorithm," *J. of Computational Physics*, Vol. 39, 1981.
26. Beam, R. and Warming, R., "An Implicit Finite-Difference Scheme for the Compressible Navier-Stokes Equations," *AIAA J,* Vol. 16, 1978, pp. 393–401.
27. Pandya, S., Chan, W., and Kless, J., "Automation of Structured Overset Mesh Generation for Rocket Geometries," AIAA Paper-2009-3993, 19th AIAA Computational Fluid Dynamics Conference, San Antonio, Texas, June 2009.
28. NAPARC Alliance- National Program for Application-Oriented Research in CFD. http://www.grc.nasa.gov/WWW/wind/.
29. Ballhaus, W. F and Goorjian, P. M., "Computation of Unsteady Transonic Flows by the Indicial Method," *AIAA J.,* Vol. 16, No. 2, Feb. 1978, pp. 117-124.
30. Ryan, R. S, "Problems Experienced and Envisioned for Dynamical Physical Systems," NASA TP-2508, 1985.
31. Guruswamy, G. P., "A Dual Level Parallel Protocol for Large Scale Computations of Aerospace Vehicles," (to be published NASA Advanced Supercomputing Division Report, NASA Ames Research Center).
32. Pleiades Computer System. (http://www.nas.nasa.gov/hecc/resources/pleiades.htm)
33. Guruswamy, G. P., "Fluid/Structure Interaction Modeling of Helicopters Using the Navier-Stokes equations," AIAA Paper 2012-4789, AIAA Modeling and Simulation Technologies Conf, Minneapolis, MN, Aug. 2012.
34. Bilstein, R. E. "Stages to Saturn – A technological History of the Apollo/Saturn Launch Vehicles," NASA SP-4206, 1996.